JACS
JOURNAL OF THE AMERICAN CHEMICAL SOCIETY
Article
pubs.acs.org/JACS

Birch Reduction of Graphite. Edge and Interior Functionalization by Hydrogen

Zhiqiang Yang,[†] Yanqiu Sun,[†] Lawrence B. Alemany,[†] Tharangattu N. Narayanan,[‡] and W. E. Billups*[,†]

[†]Department of Chemistry, Shared Equipment Authority, and The Richard E. Smalley Institute for Nanoscale Science and Technology, Rice University, 6100 Main Street, Houston, Texas 77005, United States

[‡]Department of Mechanical Engineering and Materials Science, Rice University, 6100 Main Street, Houston, Texas 77005, United States

ABSTRACT: The Birch reduction (lithium in liquid ammonia) of graphite gives a highly reduced, exfoliated product that is free of lithium. Edge and interior hydrogenation were demonstrated by solid-state ^{13}C NMR spectroscopy. Elemental analysis of a carefully purified sample allows the chemical composition to be expressed as $(C_{1.3}H)_n$. Atomic force microscopy images showed that the reduced graphene was highly exfoliated. Hydrogen mapping by electron energy loss spectroscopy showed that the entire surface of the reduced sample was covered by hydrogen, consistent with the NMR studies also indicating that hydrogen was added in interior positions of the graphene lattice as well as along the edge. A large band gap (4 eV) further establishes the high level of hydrogenation.

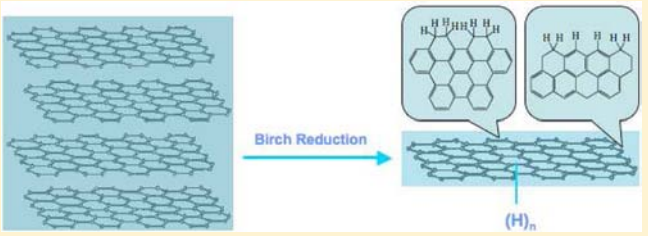

INTRODUCTION

Graphene is a two-dimensional sheet of sp^2-bonded carbon atoms that can be considered as a single atomic layer of graphite. Graphene had been studied for more than 60 years theoretically[1−3] before the real free-standing graphene was first prepared via mechanical exfoliation of graphite in 2004 by Geim and Novoselov.[4,5] This has led to a large number of studies that target potential technological applications.[6−10]

Pristine graphene is a semimetal with a zero band gap. This limits its applications in certain electronic devices where semiconductors with controllable band gaps are required. Hydrogenation provides a promising pathway to introduce a band gap into pristine graphene and thus extend its potential applications. Fully hydrogenated graphene, graphane $(CH)_n$, was theoretically predicted by Sofo and co-workers[11] and then experimentally tested more recently by Geim et al.[12] In graphane sheets, the carbon hybridization is completely transformed from sp^2 to sp^3, resulting in an insulator without any conducting π-electrons. On the other hand, partially hydrogenated graphene is a semiconductor with tunable band gaps. Conductivity depends on the C/H ratio and the distribution and ordering of H atoms as well as other effects.[13−15]

The venerated Birch reduction has been used to functionalize buckminsterfullerene, large fullerenes, carbon nanotubes, charcoal, and coals.[16−24] In this paper, we report that graphite powder can be reduced via a Birch reduction using lithium−liquid ammonia to yield highly exfoliated hydrogenated graphene that is functionalized along the edges by methylene groups. An earlier study using a similar strategy gave material with multiple layers (>40).[25]

EXPERIMENTAL SECTION

Materials. Graphite (powder, synthetic, <20 μm), lithium (granule, high sodium, 99%), and tert-butyl alcohol(anhydrous, 99.5%) were all purchased from Aldrich.

Synthesis. A 250 mL three-neck round-bottom flask equipped with a condenser was flame-dried under vacuum, flushed with argon, and then maintained under an atmosphere of argon. A dry ice−acetone mixture (−78 °C) was then applied to cool the flask and condenser. Ammonia (160 mL) was condensed into the flask, followed by the addition of lithium (960 mg, 138 mmol) and graphite (160 mg, 13.3 mmol). The mixture was stirred moderately for 1 h under the protection of argon. The dry ice−acetone bath was then removed, and tert-butyl alcohol (7 mL, 73.2 mmol) was added to the reaction mixture. The reaction mixture was refluxed at the boiling temperature of liquid ammonia (−33 °C) and stirred moderately for 4 h while refilling the dry ice−acetone condenser as needed. The ammonia in the system was then allowed to evaporate overnight. The reaction was quenched by slow addition of ethanol followed by water. After acidification with 10% HCl, the products were extracted into hexane and washed several times with water using a separatory funnel. The hexane suspension was then filtered through a 0.2 μm PTFE membrane and washed successively with hexane and ethanol. The filter cake was then redispersed into 60 mL of ethanol and ultrasonicated for 1 h. After filtration, the obtained black material was dried at 80 °C overnight under vacuum.

Characterization. The hydrogenated sample was characterized by Raman spectroscopy, powder X-ray diffraction (XRD), thermal gravimetric analysis (TGA), Fourier transform infrared spectroscopy (FTIR), atomic force microscopy (AFM), X-ray photoelectron spectroscopy (XPS), high-resolution transmission electron microscopy (HRTEM) equipped with electron energy loss spectroscopy (EELS),

Received: July 25, 2012
Published: October 17, 2012

dx.doi.org/10.1021/ja3073116 | J. Am. Chem. Soc. 2012, 134, 18689−18694

and solid-state ^{13}C NMR spectroscopy. TGA studies were carried out under argon flow (80 mL/min) using a SDT 2960 Simultaneous DSC-TGA from TA Instruments. Samples were heated to 100 °C and held at 100 °C for 10 min to dehydrate. Then they were heated at a ramp of 10 °C/min to 700 °C. Raman spectra were collected using a Renishaw 1000 micro-Raman system equipped with a 633 nm laser source. FTIR spectra were recorded in transmission mode using a Nicolet FTIR Benchtop and Microscope System. X-ray diffraction (XRD) patterns were obtained using a Rigaku D/Max Ultima II Powder Diffractometer. AFM images were taken using a Digital Instruments Nanoscope IIIA atomic force microscope in tapping mode. Samples were prepared by spin-coating suspensions (in chloroform) on mica. A Physical Electronics (PHI QUANTERA) XPS/ESCA system was used to acquire the XPS data. The base pressure of the system was 5×10^{-9} Torr. A monochromatic Al X-ray source at 100 W was used with pass energy of 26 eV and a 45° takeoff angle. The beam diameter was 100.0 μm. HRTEM images were recorded using a JEOL 2100 field emission TEM operated at an accelerating voltage of 200 kV. A drop of sample suspension in chloroform was placed on a lacey TEM grid and then dried in the air. The MAS ^{13}C NMR spectra were acquired on a Bruker AVANCE-200 NMR spectrometer (50.3 MHz ^{13}C; 200.1 MHz ^{1}H). Chemical shifts are relative to glycine carbonyl defined as 176.46 ppm.[26]

RESULTS AND DISCUSSION

The Birch reduction of graphite to yield hydrogenated graphene (graphane) is illustrated in Scheme 1.

Scheme 1. Birch Reduction of Graphite

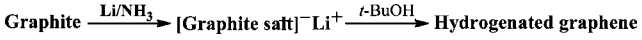

The Raman spectra of the pristine graphite and the reduced graphene are shown in Figure 1, parts a and b, respectively. The

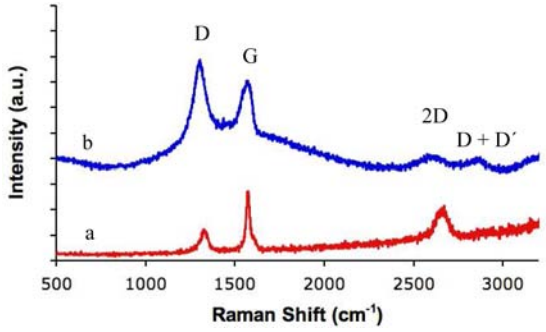

Figure 1. Raman spectra of (a) pristine graphite, and (b) hydrogenated graphene, showing changes at D, G, 2D, and (D + D′) bands.

large D band observed at 1320 cm^{-1} (Figure 1b) is indicative of the chemical disruption of the sp^2-hybridized carbon network that results from the covalent attachment of hydrogen atoms.[14] In addition, a decrease and broadening of the 2D band (also called the G′ band) at 2680 cm^{-1} and an increase of the (D + D′) combination band at 2890 cm^{-1} were also observed. Similar changes were observed when graphene was reduced by a hydrogen plasma.[12]

The FTIR spectrum of the hydrogenated sample (Figure 2b) exhibits a strong peak at 2850 cm^{-1}, indicative of the aliphatic C−H stretching mode. No peaks were observed in this region for the pristine graphite (Figure 2a).

Thermal gravimetric analyses are presented in Figure 3. The pristine graphite shows a negligible weight loss up to 700 °C,

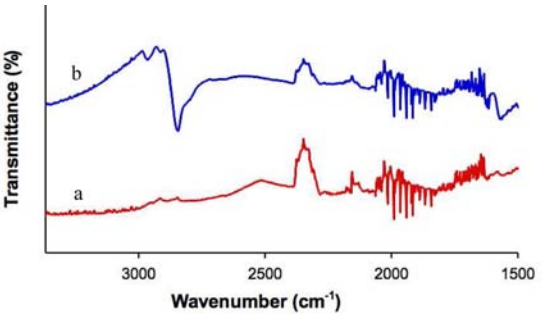

Figure 2. FTIR spectra of (a) pristine graphite, and (b) hydrogenated graphene.

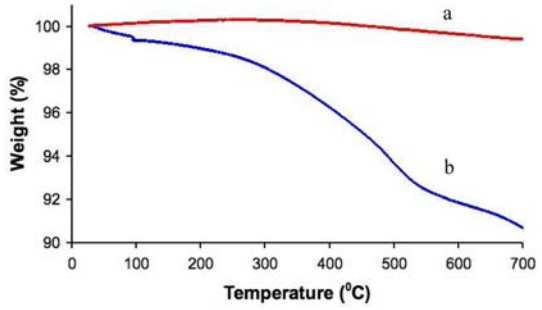

Figure 3. TGA curves of (a) pristine graphite, and (b) hydrogenated graphene.

whereas the hydrogenated sample displays a total weight loss of 10% over this temperature range. The hydrogen content of graphane $(CH)_n$ is 7.7 wt % with the release of hydrogen occurring mainly above 400 °C. If the weight loss below 400 °C is attributed to the release of adsorbed species such as alcohol and ammonia,[25] the weight loss due to the release of hydrogen is about 6%, in agreement with the elemental analysis of a carefully dried sample that shows 5.8% hydrogen by weight. This allows the chemical composition of the hydrogenated sample to be expressed as $(C_{1.3}H)_n$. A previous study using the Birch reduction but with different experimental parameters gave a hydrogenated product with formula $(C_5H)_n$.[25]

The band gap of the hydrogenated sample was determined to be ~4 eV by using UV−vis spectroscopy and Tauc's equation (Figure 4).[27] Values were measured at three concentrations using chloroform as the dispersing medium. The large band gap emphasizes the high level of hydrogenation. The sharp change in the spectrum at ~3.6 eV (~350 nm) results from the lamp change in the spectrophotometer.

MAS ^{13}C NMR experiments (Figure 5) provide additional evidence of reduction and further indicate that the hydrogen is not uniformly distributed. A $^{1}H-^{13}C$ CPMAS spectrum (Figure 5a) shows a relatively strong aliphatic signal compared to the aromatic signal. In contrast, direct ^{13}C pulse MAS spectra show a proportionately stronger aromatic carbon signal whose intensity steadily increases as the relaxation delay is lengthened up to 180 s (Figure 5d, 5e, and 5f). Clearly, there are slowly relaxing aromatic carbon nuclei that are presumably in the more interior positions of condensed aromatic ring systems and thus cannot efficiently relax through dipolar processes (or be cross-polarized in the CP experiment[28,29]). At the low field strength used (50.3 MHz ^{13}C), relaxation via chemical shift anisotropy (CSA) is also limited. Even with only some of the carbons detected in the CP spectrum, its S/N is much higher, reflecting

dx.doi.org/10.1021/ja3073116 | J. Am. Chem. Soc. 2012, 134, 18689−18694

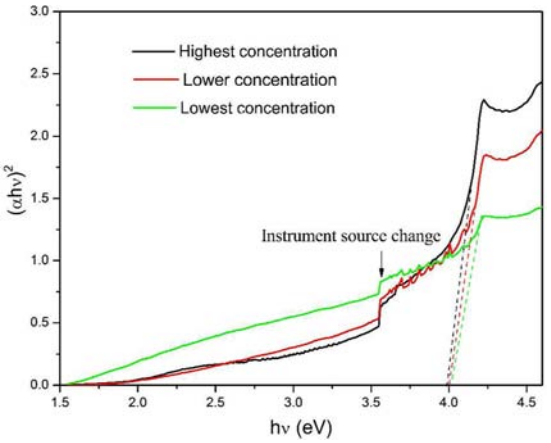

Figure 4. Band gap of hydrogenated graphene. Three samples with different concentrations in chloroform were measured with UV−vis spectroscopy and then plotted using Tauc's equation. The extrapolated dashed lines indicate a band gap of 4 eV.

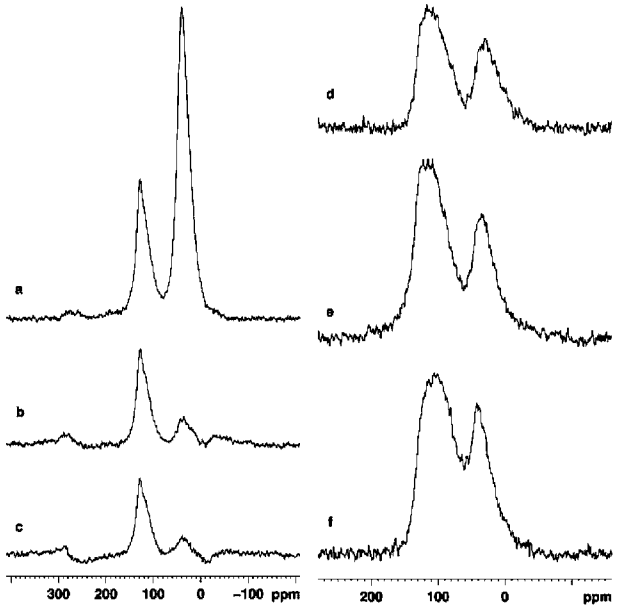

Figure 5. MAS ^{13}C NMR spectra of hydrogenated graphene. All FIDs were processed with 50 Hz (1 ppm) of line broadening. (a) $^{1}H-^{13}C$ CPMAS spectrum obtained with 7.6 kHz spinning, a contact time of 1 ms, and a relaxation delay of 5 s (15 000 scans). Weak aromatic spinning sidebands are evident. (b) As in spectrum a, but with a 50-μs dephasing interval between cross-polarization and FID acquisition. (c) As in spectrum a, but with an 80-μs dephasing interval between cross-polarization and FID acquisition. Spectra a−c are plotted with the same level of baseline noise to facilitate comparison. (d−f) 90° ^{13}C pulse MAS spectra obtained with 12 kHz spinning and baseline correction (standard Bruker software) to remove curvature: (d) relaxation delay of 30 s and 2800 scans, (e) relaxation delay of 90 s and 2800 scans, (f) relaxation delay of 180 s and 1336 scans. To facilitate comparison, spectra d and e are plotted with the same level of baseline noise, and spectra e and f are plotted with the same height for the aromatic carbon band.

the well-known sensitivity enhancement for the carbon signals detected by cross-polarization as well as much shorter spin−lattice relaxation times for the protons than for the ^{13}C nuclei.

In the direct ^{13}C pulse spectra (Figure 5d−f), the peak maxima are at least 10 ppm upfield of the peak maxima in the CP spectrum, again demonstrating that the carbon environment near protons is significantly different from the carbon environment far from protons. Indeed, the direct ^{13}C pulse spectra exhibit a significant amount of unusually shielded aromatic carbon. This is particularly apparent in the spectrum obtained with a 180-s relaxation delay. The unusual shielding can be attributed to the diamagnetic shift in the δ_{33} component of the shielding tensor of the numerous bridgehead carbons in a large condensed aromatic ring system[30] and thus indicates the presence of regions of unreacted condensed aromatic ring systems in hydrogenated graphene. Two prior reports are particularly relevant: the very shielded carbon signal observed for highly reduced graphite oxide (a broad aromatic carbon signal with a maximum at δ 105 in a 50 MHz ^{13}C spectrum of chemically converted graphene CCG3)[31] and the even more shielded aromatic carbon signal observed for 20 wt % graphite dispersed in silica (a much broader signal with a maximum at δ 72 in a 25 MHz ^{13}C, 864-scan spectrum obtained with a 600-s relaxation delay).[29,30] An appreciation for just how shielded the aromatic carbons are in these two materials can be gained by considering chemical shifts in model compounds. The six equivalent carbons in the center ring of coronene (δ 121) are considerably more shielded than the bridgehead carbons in anthracene (δ 132), while the even more interior carbons in circumcoronene have calculated chemical shifts of δ 117 (the most interior position) and δ 119.[32]

The very shielded aromatic carbon nuclei in graphite[29,30] and hydrogenated graphene clearly relax very slowly for the reasons noted above. (The CSA contribution to relaxation is even smaller at 25 MHz ^{13}C.) The S/N in the 1336-scan spectrum of hydrogenated graphene obtained with a 180-s relaxation delay (Figure 5f) is similar to that obtained in the 2800-scan spectrum with only a 90-s relaxation delay (Figure 5e). Relaxation may not yet be complete even with a 180-s relaxation delay.

Highly conductive samples present problems in tuning the NMR probe.[28] The entirely aromatic chemically converted graphene CCG3 greatly affected the tuning and matching characteristics of the ^{13}C and ^{1}H channels in the probe.[31] In contrast, the significant structural alteration in hydrogenated graphene results in only moderate adjustments (compared to glycine) for tuning and matching the ^{13}C and ^{1}H channels in the probe. This structural change also explains why it is not necessary to disperse hydrogenated graphene in a non-conductive solid (e.g., silica), as is necessary for graphite (and, as recently reported, for conductive, edge-functionalized, hexadecylated graphene nanoribbons[33]) in order to tune the probe and obtain a spectrum.

Inserting a 50-μs dephasing interval between cross-polarization and FID acquisition[24] greatly attenuates, but does not eliminate, the aliphatic signal (Figure 5b). Lengthening the interval to 80 μs only moderately further weakens the aliphatic signal (Figure 5c). Quaternary aliphatic carbons and methyl carbons, which would give relatively slowly decaying signals, clearly cannot be present in hydrogenated graphene. The rigid structural environment for the interior aliphatic CH groups (at the junction of three rings in a fused ring system) would be expected to result in strong $^{13}C-^{1}H$ dipole−dipole interactions that would result in complete or virtually complete decay of the aliphatic CH signals with a 50-μs dephasing interval. If hydrogen addition occurred only on the periphery, a very large, presumably still highly conductive, polynuclear aromatic ring system would still remain, and problems in tuning and

dx.doi.org/10.1021/ja3073116 | J. Am. Chem. Soc. 2012, 134, 18689−18694

matching the ^{13}C and ^{1}H channels in the probe would still be expected. As noted above, hydrogenated graphene does not present such problems. Thus, one can reasonably conclude that some hydrogen addition occurs in interior positions of graphite, which would severely reduce the conductivity of the hydrogenated graphene.

The small amount of aliphatic intensity that remains even after an 80-μs dephasing interval may result from CH_2 groups on the periphery in rings that have more motional freedom, resulting in weaker $^{13}C-^{1}H$ dipole–dipole interactions. In this context, we note that dipolar dephasing experiments on some low-rank coals have provided evidence for segmental motion thought to arise from CH_2 groups associated with hydroaromatic and/or polymethylene structural units.[34] Unfortunately, we do not have any suitable solid hydroaromatic model compounds to study for comparison. The proportionately much smaller decay of the aromatic signal in the dipolar dephasing experiment is reasonable; the decay mostly reflects the loss of signal from the aromatic CH groups, as the signals from the quaternary aromatic carbons decay much more slowly.

A recent study on the Billups–Birch reductive alkylation of single-walled carbon nanotubes pointed out that the alkylation did not take place randomly on the graphene lattices of the tubes.[35] Instead, it preferred to happen at defect sites and then propagated exclusively from those sites, which resulted in clustered distribution of the functional groups. The NMR results discussed above imply that the Birch hydrogenation of graphite layers may follow the same way, leaving unreacted islands on the lattices when the hydrogenation is not complete.

The identification of methylene groups (CH_2) can only be rationalized in terms of edge functionalization by hydrogen. The introduction of methylene groups into the basal plane is unlikely because it would require cleavage of the graphene network. Edge functionalization of graphene ribbons has been investigated theoretically for both zigzag and armchair edges.[36] Structures **1** and **2** are consistent with the calculations and would be derived from zigzag and armchair edges, respectively. It is important that any scheme leading to edge functionalization obey Clar's rule,[37] which requires that each benzene ring shall be accommodated by a sextet of electrons.

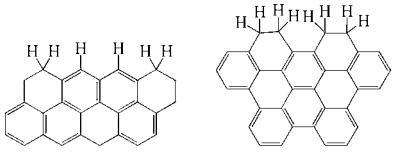

1 **2**

The C1s X-ray photoelectron spectroscopy (XPS) patterns of the pristine graphite and the hydrogenated sample are given in Figure 6. The spectra are normalized for clear comparison. The pristine graphite shows a relatively narrow peak at 284.5 eV that can be assigned to sp^2-hybridized carbon. The Birch reduction leads to a large amount sp^3-hybridized carbon. As a result, the XPS pattern of the reduced sample shows a broadened C1s peak that contains both sp^2 and sp^3 components. Similar broadening of the C1s peak was reported recently for irradiation-induced hydrogenated graphene.[38] We were pleased to find that only a small amount of Li (less than 0.2 atom %) remained in the product.

X-ray diffraction patterns are presented in Figure 7. The XRD pattern of the graphite (Figure 7a, blue line) exhibits a sharp diffraction peak at 2θ = 26.32°, corresponding to the

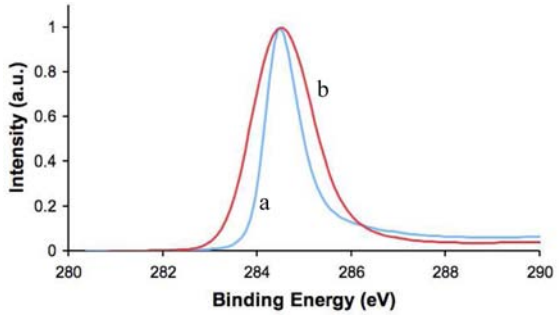

Figure 6. C1s XPS spectra of pristine graphite (a, blue line) and hydrogenated graphene (b, red line). The spectra are normalized for comparison.

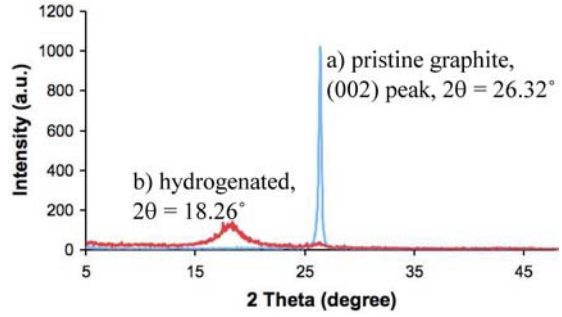

Figure 7. Powder XRD patterns of pristine graphite (a, blue line) and hydrogenated graphene (b, red line). Notice the substantial decrease of the (002) peak and the appearance of a new broad peak after the Birch reduction.

(002) crystal planes of graphite with a layer distance of 3.38 Å. The XRD pattern of the reduced sample (Figure 7b, red line) exhibits a broad new peak at 2θ = 18.26°, indicating an interplanar spacing of 4.90 Å. The spacing increase from 3.38 Å to 4.90 Å is attributed to the covalently bound hydrogen atoms on the surface of the exfoliated graphene. Using the density functional theory and the van der Waals density functional method, the binding separation (distance between center-of-mass planes) of graphane was calculated to be 4.5–5.0 Å.[39] This is consistent with the interplanar spacing (4.90 Å) that we observe for the Birch-reduced sample.

The width (broad) and the low intensity of the peak exhibited by the reduced sample imply poor crystallization, i.e., the exfoliation of the original layered structure. Atomic force microscopy (AFM) measurements were carried out to determine the shape and thickness of the hydrogenated sample. The sample was dispersed in chloroform and spin-coated onto mica for the AFM measurements. A typical AFM image (5 × 5 μm) in tapping mode is given in Figure 8a. It shows irregular-shaped sheets with horizontal sizes varying from 0.2 to 3 μm and an average height around 0.5 nm (see the color bar in Figure 8a). In Figure 8b, a typical section analysis indicates the step height of the surface where the white line in Figure 8a crosses several sheets. The two red triangles in Figure 8a and 8b exhibit the AFM tip on or off one sheet, and the corresponding height change is 0.4 nm. These results indicate that the original graphite was highly exfoliated during the Birch reduction.

The SEM image of the hydrogenated sample shows crumpled sheets (Figure 9a). The HRTEM images of the reduced sample also appear as crumpled sheets when observed at high magnification (Figure 9b,c). A more enlarged image

dx.doi.org/10.1021/ja3073116 | J. Am. Chem. Soc. 2012, 134, 18689–18694

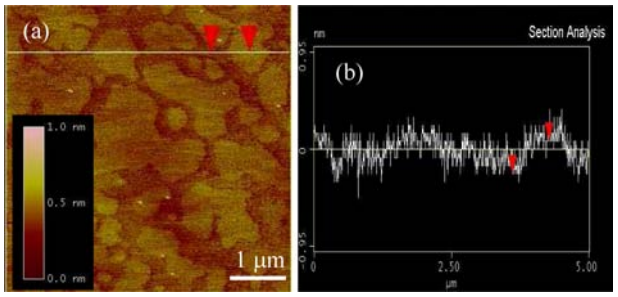

Figure 8. AFM measurement of the hydrogenated sample, demonstrating the high exfoliation of the original graphite after the Birch reduction. (a) Tapping mode image (5 × 5 μm), inset: color bar depicts the height. (b) AFM section analysis, indicating the step height of the surface where the white line in panel a crosses several sheets.

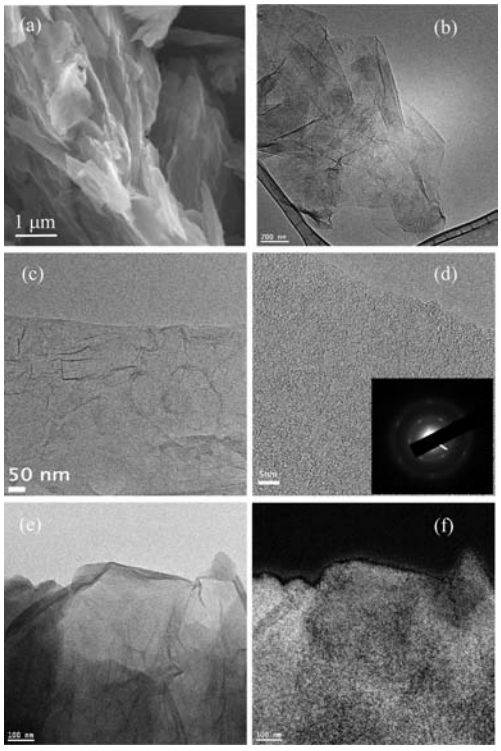

Figure 9. (a) SEM image of the hydrogenated graphene. (b, c) Typical HRTEM images with different magnification. Scale bar in panel b: 200 nm. (d) HRTEM image at highest magnification, plus the selected area electron diffraction pattern as the inset. Scale bar: 5 nm. (e) An image shows the region used for the hydrogen mapping. Scale bar: 100 nm. (f) Hydrogen mapping obtained by electron energy loss spectroscopy. Scale bar: 100 nm.

indicates that it is a single layer (Figure 9d). The selected area electron diffraction pattern shows that the hexagonal two-dimensional crystal structure of graphene remains after the Birch reduction.[12] Electron energy loss spectroscopy was also applied to indicate the hydrogen distribution of the reduced sample. Figure 9e shows the region used for the hydrogen mapping, and Figure 9f shows that the entire surface is covered by hydrogen. Covering the entire surface implies that hydrogen is added in interior positions of the graphene lattice as well as along the edge, consistent with the inference drawn from the NMR studies (discussed above) where tuning and matching of the ^{13}C and ^{1}H channels proved to be uneventful.

CONCLUSIONS

Commercially available graphite powder was hydrogenated using lithium in liquid ammonia with tert-butyl alcohol as the source of protons. High exfoliation was demonstrated by X-ray diffraction, atomic force spectroscopy, and electron microscopy. The reduced graphene was determined to be $(C_{1.3}H)_n$ by elemental analysis. Several analytical studies further demonstrated the high level of hydrogenation. The high level of reduction allowed solid-state ^{13}C NMR studies to be carried out and used to identify edge and interior hydrogenation. Hydrogen mapping by electron energy loss spectroscopy showed that the entire surface of the reduced graphene is covered by hydrogen. Of particular significance, analysis of the UV−vis spectrum of the hydrogenated graphene indicated a large band gap of ∼4 eV.

AUTHOR INFORMATION

Corresponding Author

billups@rice.edu

Notes

The authors declare no competing financial interest.

ACKNOWLEDGMENTS

We gratefully acknowledge the Robert A. Welch Foundation for supporting this work. Funding for the upgrade of the 200 MHz NMR spectrometer was provided through NSF award CHE0947054.

REFERENCES

(1) Wallace, P. R. *Phys. Rev.* **1947**, *71*, 622.
(2) McClure, J. W. *Phys. Rev.* **1956**, *104*, 666.
(3) (a) Slonczewski, J. C.; Weiss, P. R. *Phys. Rev.* **1958**, *109*, 272. (b) Hummers, W. S.; Offeman, R. E. *J. Am. Chem. Soc.* **1958**, *80*, 1339.
(4) Novoselov, K. S.; Geim, A. K.; Morozov, S. V.; Jiang, D.; Zhang, Y.; Dubonos, S. V.; Grigorieva, I. V.; Firsov, A. A. *Science* **2004**, *306*, 666.
(5) Novoselov, K. S.; Jiang, D.; Schedin, F.; Booth, T. J.; Khotkevich, V. V.; Morozov, S. V.; Geim, A. K. *Proc. Natl. Acad. Sci. U.S.A.* **2005**, *102*, 10451.
(6) (a) Huang, X.; Yin, Z.; Wu, S.; Qi, X.; He, Q.; Zhang, Q.; Yan, Q.; Boey, F.; Zhang, H. *Small* **2011**, *7*, 1876. (b) Zeng, Z.; Yin, Z.; Huang, X.; Li, H.; He, Q.; Lu, G.; Boey, F.; Zhang, H. *Angew. Chem., Int. Ed.* **2011**, *50*, 11093. (c) Huang, X.; Qi, X.; Boey, F.; Zhang, H. *Chem. Soc. Rev.* **2012**, *41*, 666. (d) He, Q.; Wu, S.; Yin, Z.; Zhang, H. *Chem. Sci.* **2012**, *3*, 1764.
(7) Pang, S.; Hernandez, Y.; Feng, X.; Muellen, K. *Adv. Mater.* **2011**, *23*, 2779.
(8) Zhang, Y.; Tan, Y. W.; Stormer, H. L.; Kim, P. *Nature* **2005**, *438*, 201.
(9) Novoselov, K. S.; Geim, A. K.; Morozov, S. V.; Jiang, D.; Katsnelson, M. I.; Grigorieva, I. V.; Dubonos, S. V.; Firsov, A. A. *Nature* **2005**, *438*, 197.
(10) Heersche, H. B.; Jarillo-Herrero, P.; Oostinga, J. B.; Vandersypen, L. M. K.; Morpurgo, A. F. *Nature* **2007**, *446*, 56.
(11) Sofo, J. O.; Chaudhari, A. S.; Barber, G. D. *Phys. Rev. B* **2007**, *75*, 153401.
(12) Elias, D. C.; Nair, R. R.; Mohiuddin, T. M. G.; Morozov, S. V.; Blake, P.; Halsall, M. P.; Ferrari, A. C.; Boukhvalov, D. W.; Katsnelson, M. I.; Geim, A. K.; Novoselov, K. S. *Science* **2009**, *323*, 610.
(13) Matis, B. R.; Burgess, J. S.; Bulat, F. A.; Friedman, A. L.; Houston, B. H.; Baldwin, J. W. *ACS Nano* **2012**, *6*, 17.
(14) Jaiswal, M.; Lim, C. H.; Bao, Q.; Toh, C. T.; Loh, K. P.; Ozyilmaz, B. *ACS Nano* **2011**, *5*, 888.
(15) Gao, H.; Wang, L.; Zhao, J.; Ding, F.; Lu, J. *J. Phys. Chem. C* **2011**, *115*, 3236.

(16) Haufler, R. E.; Conceicao, J.; Chibante, L. P. F.; Chai, Y.; Byrne, N. E.; Flanagan, S.; Haley, M. M.; O'Brien, S. C.; Pan, C.; Xiao, Z.; Billups, W. E.; Ciufolini, M. A.; Hauge, R. H.; Margrave, J. L.; Wilson, L. J.; Curl, R. F.; Smalley, R. E. *J. Phys. Chem.* **1990**, *94*, 8634.
(17) Nossal, J.; Saini, R. K.; Sadana, A. K.; Bettinger, H. F.; Alemany, L. B.; Scuseria, G. E.; Billups, W. E.; Saunders, M.; Khong, A.; Weisemann, R. *J. Am. Chem. Soc.* **2001**, *123*, 8482.
(18) Borondics, F.; Jakab, E.; Pekker, S. *J Nanosci. Nanotechnol.* **2007**, *7*, 1551.
(19) Liang, F.; Sadana, A. K.; Peera, A.; Chattopadhyay, J.; Gu, Z.; Hauge, R. H.; Billups, W. E. *Nano Lett.* **2004**, *4*, 1257.
(20) Liang, F.; Alemany, L. B.; Beach, J. M.; Billups, W. E. *J. Am. Chem. Soc.* **2005**, *127*, 13941.
(21) Mukherjee, A.; Alemany, L. B.; Chattopadhyay, J.; Chakraborty, S.; Guo, W.; Yates, S. M.; Billups, W. E. *Chem. Mater.* **2008**, *20*, 5513.
(22) Mukherjee, A.; Alemany, L. B.; Thaner, R.; Guo, W. H.; Billups, W. E. *Carbon* **2009**, *47*, 3145.
(23) Sun, Y.; Mukherjee, A.; Kuznetsov, O.; Thaner, R.; Alemany, L. B.; Billups, W. E. *Energy Fuels* **2011**, *25*, 1571.
(24) Sun, Y.; Kuznetsov, O.; Alemany, L. B.; Billups, W. E. *Energy Fuels* **2011**, *25*, 3997.
(25) Pekker, S.; Salvetat, J. P.; Jakab, E.; Bonard, J. M.; Forro, L. *J. Phys. Chem. B* **2001**, *105*, 7938.
(26) Hayashi, S.; Hayamizu, K. *Bull. Chem. Soc. Jpn.* **1991**, *64*, 685.
(27) (a) Ci, L.; Song, L.; Jin, C.; Jariwala, D.; Wu, D.; Li, Y.; Srivastava, A.; Wang, Z. F.; Storr, K.; Balicas, L.; Liu, F.; Ajayan, P. M. *Nat. Mater.* **2010**, *9*, 430. (b) Song, L.; Ci, L.; Lu, H.; Sorokin, P. B.; Jin, C.; Ni, J.; Kvashnin, A. G.; Kvashnin, D. G.; Lou, J.; Yakobson, B. I.; Ajayan, P. M. *Nano Lett.* **2010**, *10*, 3209.
(28) Solum, M. S.; Sarofim, A. F.; Pugmire, R. J.; Fletcher, T. H.; Zhang, H. *Energy Fuels* **2001**, *15*, 961.
(29) Jiang, Y. J.; Solum, M. S.; Pugmire, R. J.; Grant, D. M. *Energy Fuels* **2002**, *16*, 1296.
(30) Pugmire, R. J.; Solum, M. S.; Jiang, Y. J.; Sarofim, A. F.; Veranth, J.; Schobert, H. H.; Pappano, P. J. *Prepr. Symp. − Am. Chem. Soc., Div. Fuel Chem.* **2002**, *47* (2), 733.
(31) Gao, W.; Alemany, L. B.; Ci, L.; Ajayan, P. M. *Nat. Chem.* **2009**, *1*, 403.
(32) Orendt, A. M.; Facelli, J. C.; Bai, S.; Rai, A.; Gossett, M.; Scott, L. T.; Boerio-Goates, J.; Pugmire, R. J.; Grant, D. M. *J. Phys. Chem. A* **2000**, *104*, 149.
(33) Genorio, B.; Lu, W.; Dimiev, A. M.; Zhu, Y.; Raji, A.-R. O.; Novosel, B.; Alemany, L. B.; Tour, J. M. *ACS Nano* **2012**, *6*, 4231.
(34) Soderquist, A.; Burton, D. J.; Pugmire, R. J.; Beeler, A. J.; Grant, D. M.; Durand, B.; Huk, A. Y. *Energy Fuels* **1987**, *1*, 50.
(35) Deng, S.; Zhang, Y.; Brozena, A. H.; Mayes, M. L.; Banerjee, P.; Chiou, W. A.; Rubloff, G. W.; Schatz, G. C.; Wang, Y. *Nat. Commun.* **2011**, *2*, 382.
(36) Wassmann, T.; Seitsonen, A. P.; Saitta, A. M.; Lazzeri, M.; Mauri, F. *Phys. Rev. Lett.* **2008**, *101*, 096402.
(37) Clar, E. *The Aromatic Sextet*: Wiley, New York, 1972.
(38) Chen, W.; Zhu, Z.; Li, S.; Chen, C.; Yan, L. *Nanoscale* **2012**, *4*, 2124.
(39) Rohrer, J.; Hyldgaard, P. *Phys. Rev. B* **2011**, *83*, 165423.